Carbon 238 (2025) 120304

Contents lists available at ScienceDirect

Carbon

journal homepage: www.elsevier.com/locate/carbon

Radio frequency (RF) enabled forming of vitrimers for moldless manufacturing

Agni K. Biswal [a,1], Surabhit Gupta [a,1], Xu Zhou [b], Thomas K. Lewis [a], Juming Tang [b], Aniruddh Vashisth [a,*]

[a] Mechanical Engineering, University of Washington, Seattle, WA, 98195, USA
[b] Industrial & Systems Engineering, University of Washington, Seattle, WA, 98195, USA

ARTICLE INFO

Keywords:
Vitrimers
Advanced manufacturing
Forming
RF heating
Moldless manufacturing

ABSTRACT

The need for efficient, sustainable manufacturing methods has driven significant interest in vitrimer-based composites, known for their reprocessability and dynamic covalent networks. Here, we present a new moldless manufacturing method using radio frequency (RF) heating to reshape vitrimer composites. Two transesterification vitrimer polymer systems with distinct thermal properties were synthesized, incorporating bifunctional and tetra-functional epoxides to tune rigidity. Optimal RF heating was achieved by incorporating 3 wt% carbon black in the polymers, enabling rapid, localized heating and efficient deformation of vitrimer plates. Additionally, multi-physics simulations were performed to correlate the relation between conductive filler percentage and RF heating. The RF-forming process demonstrated successful reshaping of vitrimers at temperatures above the glass transition temperatures, resulting in stable structures without using molds. Furthermore, the two vitrimer composite samples were RF-formed and welded together; welding was done at topological freezing temperature of vitrimers to ensure covalent bonds at the interface. This study reveals the potential of RF heating and forming as an energy-efficient, moldless technique for rapid prototyping and reprocessing of vitrimer-based composites, offering a promising alternative for advanced manufacturing applications.

1. Introduction

Processing and fabrication of polymers and their composites are experiencing rapid growth, with an estimated market value of $144.5 billion by 2028 [1]. This growth is driven by the increasing adoption of polymers in several industries such as electronics, automotive, and medical devices. Thermoplastics have gained traction for their recyclability, ease of processing, impact resistance, and repairability. Traditional methods for manufacturing and processing thermoplastic or thermosetting polymers [2,3] include compression molding, injection molding, blow molding, rotational molding, extrusion, thermoforming, and incremental forming. [2,3]. With a recent push towards sustainability, a wide range of work is being done on manufacturing and processing of polymers with covalent adaptable networks (CANs) that have unique properties like self-healing and shape-memory vitrimers [4–6].

Polymers with CANs can change their network topology in response to external stimuli. CANs can be categorized into two types: dissociative CANs [7–9] and associative CANs [10]. Associative CANs are particularly promising since these polymers maintain their integrated structure when the reversible covalent bonds break by ensuring a constant crosslink density in the network. In 2011, Leibler and co-workers created epoxy *vitrimers using associative CANs*, incorporating transesterification catalysts into epoxy/acid or epoxy/anhydride polyester networks [10]. Since their inception, various exchangeable reactions have been discovered and explored, including transesterification [11], disulfide exchange [12], transalkylation exchange [13] and many more [14–16]. These materials are termed vitrimers since their viscosity behaviour approaching the glass transition temperature (T_g) follows an Arrhenius law and is analogous to vitreous silica. Vitrimers are characterized by a topology freezing transition temperature (T_v), above which the reversible crosslinking reaction can be achieved at higher rates, enabling self-healing capabilities and reprocessability [17,18]. Typically, vitrimers exhibit $T_v > T_g$; this is exciting as most applications of polymers are below or close to T_g. Most of the previous work has

* Corresponding author.
E-mail address: vashisth@uw.edu (A. Vashisth).
[1] Equal Contribution by authors.

https://doi.org/10.1016/j.carbon.2025.120304
Received 15 February 2025; Received in revised form 3 April 2025; Accepted 5 April 2025
Available online 5 April 2025

focused on either vitrimer processing and crosslinking [19–21], or on crosslinked vitrimer healing [22], bonding [23,24], recycling [25], and disassembly-reassembly [26,27].

As polymer composites and vitrimers are finding widespread applications, a need for rapid prototyping structures has emerged. All traditional methods of manufacturing composites require dies or mold for a desired geometry; fabrication of dies and molds through machining is expensive and time-consuming and becomes the bottleneck when designing and manufacturing prototypes. Polymer forming techniques are low-cost methods as they require little or no molds for manufacturing. In thermoforming, plastic sheets are formed over a single mold at elevated temperatures and pressure [28], whereas in incremental forming [29,30] a material sheet is deformed into desired shape through a series of controlled movements without the need for a dedicated die. [30,31] In both of these methods, polymers are heated below melting temperatures to achieve softening but not flowability, this ensures that the polymer chains can be deformed or stretched under stress into desired shapes [28,32]. Upon cooling, the polymer network sets into a permanent shape. Forming operations are done on thermoplastics, as thermosets have a set network that inhibits chain movement. To date, forming of vitrimer polymers has not been attempted or studied. The two requirements for forming materials are pressure and temperature: localized pressure can be applied by “pinching" polymeric sheets using robots, and a new method of RF heating can be used for targeted, energy-efficient, and localized heating.

Recently, it was discovered that carbonaceous material systems heat in response to electric fields in the RF range (1–200 MHz) [33]. The RF heating response of composites with carbonaceous fillers depends on the material dielectric properties and the electric field intensity and frequency. Polymers can be reinforced by conducting fillers such as CB, carbon fibers, and graphene, and the electrical properties and resulting RF heating of these composites can be tuned as a function of filler concentrations [34,35]. Compared to conventional processing methods, RF heating provides energy-efficient, non-contact, out-of-oven heating. Compared to traditional thermal processing techniques, RF heating is energy-efficient, non-contact, and out-of-oven. Unlike induction heating, which demands closed-loop applicators and high power inputs [36], resistive heating, which necessitates direct contact [37], or microwave heating, which often results in uneven heating and requires stringent safety measures [38], RF heating penetrates deeper and provides selective heating tailored by material composition [39]. Thus, RF heating is particularly advantageous for moldless manufacturing, enabling rapid prototyping and efficient shaping of polymeric systems like vitrimers.

In this work, we developed a custom-built RF-forming machine that integrates localized RF heating with controlled actuation to form vitrimer composites into complex shapes without dies or molds. We also explored the method’s effectiveness on two vitrimer systems with different thermo-mechanical properties and demonstrated the application in welding different vitrimer chemistries through transesterification rearrangement reactions. Additionally, we developed a multi-physics simulation model explaining the RF heating response of carbon black-reinforced vitrimer composites.

2. Methods

2.1. Materials for polymer synthesis

The required materials for synthesis of vitrimer polymers, such as adipic acid, 4,4′-Methylenebis(N,N-diglycidylaniline)(Tetrafunctional epoxide), and catalyst 1,5,7-Triazabicyclo[4.4.0]dec-5-ene (TBD) were purchased from Sigma Aldrich. Diglycidyl ether of Bisphenol A (DGEBA) epoxide (EPON 828, bifunctional epoxide) was purchased from Sky-Geek, USA. RF susceptor carbon black (100% compressed, surface area: 80 m^2/g) was procured from Alfa Aesar. Solvents toluene and acetone were procured from Fischer Scientific. Other lab consumables, including adhesive Teflon sheets and high-temperature Kapton tape were purchased from McMaster.

2.2. Synthesis of vitrimer polymers

To show the flexibility of RF-forming method for applicability for different systems, we synthesized two vitrimers with different glass transition temperatures (T_g), in line with our previous work [23,40]. The fabrication process is depicted in Fig. S1. For the first vitrimer, we used 1:1 equivalent molar stoichiometric amount of adipic acid and bifunctional epoxide (EPON 828) containing 5 mol% of catalyst TBD. Initially, catalyst and epoxide were mixed using a magnetic hot plate stirrer at 120 °C for 2 min, followed by adding adipic acid; this mixture was additionally stirred for another 10–15 min to yield a clear homogenous mixture. The resulting solution was poured into a mold and kept under a vacuum for 2 min to remove air bubbles. The specimen was then heat pressed at 160 °C and cured for 7 h under 1 MPa pressure, and the system was termed V-Low (Table 1). Another set of vitrimers (V-High) containing tetra-functional epoxide and bifunctional epoxide were fabricated by keeping the polymer weight ratios at 50 wt% each. The adipic acid was added to the above mixture of epoxides with 1:1 equivalent molar ratio after adding 5 mol% catalyst TBD. The mixing and degassing of the resin mixture followed the same steps as stated above for the first vitrimer composition; however, the curing process in the heat press was carried out at 180 °C for 7 h under 1 MPa. Vitrimers with only bifunctional epoxides will have lower T_g as compared to vitrimers with a combination of bi- and tetra-functional epoxides; therefore, the former vitrimers with lower T_g are termed as V-Low, and the latter with higher T_g are termed as V-High.

Several fillers, including carbon black (CB), carbon nanotubes (CNTs), graphene, and metallic particles, have been explored as RF susceptors [39]. CB was selected in this study due to its cost-effectiveness, ease of dispersion, and broad processing viscosity range. CNTs and graphene typically pose challenges in dispersion and increased viscosity at low concentrations. Metallic particles can achieve high heating rates but significantly alter viscosity and can adversely affect mechanical properties by introducing brittleness. Therefore, CB was incorporated into the synthesized polymers to change their electrical conductivity and enhance RF heating.

Different concentrations of CB ranging from 0.1 to 5 % were added to V-Low polymers, and specimens of similar size were heated using the RF device. CB concentration was systematically optimized to achieve an optimal balance between heating efficiency and processability. CB concentration that yielded the highest change in temperature per unit time at constant power and frequency was used for making ~2.5 mm thick plates of V-Low and V-High vitrimer chemistries. These plates were stored in desiccant chambers for further characterization and RF-forming process.

2.3. RF-forming machine fabrication

RF-forming is an innovative manufacturing process that utilizes RF heating to form materials with enhanced energy efficiency compared to conventional heating methods. In this study, we employed RF-forming to process recyclable and reprocessable vitrimer materials, introducing a novel approach to advanced manufacturing. Vitrimers were selected

Table 1
Compositions for the fabricated samples.

Sample name	Epoxy content (%)		Carbon black (%)
	Bifunctional epoxide	Tetrafunctional epoxide	
V-Low	100	0	0
V-High	50	50	0
CB/V-Low	100	0	3
CB/V-High	50	50	3

due to their broad thermal transition temperature window, which is ideal for RF-forming applications.

Pressure and temperature are two key fabrication parameters to deform any polymer or its composite. To achieve this, the RF-forming machine combined a linear actuator, driver, load cell, sample holder, and RF applicator on an 80/20 aluminium extrusion frame (McMaster Carr). The linear actuator is used to achieve localized pressure; the actuator is driven by a HW 039 H-bridge driver that is controlled by an Arduino. The tip of the actuator has a 3D-printed head that houses the load cell and a glass-tipped probe to press on the material that is held by the specimen holder. We chose a glass tip for localized pinching since glass is a ceramic material, and its mechanical properties are not affected within the temperature ranges used for polymer processing. The heating mechanism in the machine uses RF heating. The RF heating system consists of a signal generator (Rigol Inc., DSG815) and a 100 W amplifier (Minicircuits ZHL-100W-GAN+) that delivers RF power to the RF applicator through a 50Ω coaxial cable. A FLIR infrared camera (FLIR Systems Inc., A400) was used to record the surface temperature during RF heating and was processed using FLIR Research Studio. An emissivity value of 0.9 was selected. Calibration was done by comparing temperature with a type K thermocouple over a temperature range of 25 °C–175 °C, with minimal differences observed. Unlike conventional heating methods, our RF-forming setup ensures precise, non-contact heating, minimizing energy loss and enabling localized material softening.

Next, we assembled the RF forming machine as shown in Fig. 1. Prior to assembly, we ensured the accuracy and reliability of the instrument by verifying key parameters such as expected loading conditions, the distance between the probe and the RF applicator, appropriate clamping for various components, and the designated heating zones. A 10 N load cell was attached to the probe head to measure the applied force during the forming experiment. Calibration of the load cell was performed using a series of known loads and measuring the resulting voltage responses (Fig. S2); these were fitted to a non-linear equation as described in the manufacturer's datasheet. Due to the small effective area of the load sensor, a freely moving piston assembly with a striking pin was employed to accurately transfer the applied load to the load cell, detailed in Fig. 1.

The rest of the machine assembly, particularly the frame constructed from aluminum extrusions and the linear actuator, was designed to be as rigid as possible to minimize mechanical deflection during operation. The sample holder and the RF applicator holder were 3D-printed with PETG, providing the flexibility to extend the system's degrees of freedom for accommodating more complex geometries and loading conditions in future iterations of the machine. Glass was chosen as the indenting material for the probe tip due to its high-temperature resistance and to minimize the use of metallic components near the RF applicator. This choice helps ensure efficient and safe heating of the material without interference from external metallic reflectors. Other parts, such as the sample stage, probe, and load cell holding components, were also 3D-printed using PETG filament (Fig. S2).

The RF applicator was positioned with an offset from the glass tip so that during RF-forming operations, the specimen was heated by the RF field. The actuator initiated deformation as heat conducted through the material (Fig. 1 inset). This offset provided a "pinching" operation on the specimen in the form of shear or bending load, depending on the boundary conditions chosen for the experiment. The offset prevents direct contact between the actuator and the RF applicator, which is designed not to move during the process. Some compliance was built into the RF applicator mounting to ensure that it does not break under the applied stress.

The entire assembly was controlled by an Arduino Uno board running custom code that monitored, through three sensors: force, displacement, and actuator state (extension, retraction, and stop). The Arduino communicated these readings in real-time to a MATLAB script running on a connected windows laptop. The MATLAB script recorded the sensor data at each time point for subsequent analysis. The RF heating system was independently controlled using another laptop running FLIR Research Studio v2024.5.0, with the heating parameters (frequency and power) manually adjusted on the signal generator. Fig. S10 shows the control diagram for the whole machine.

2.4. Polymer characterization

Thermo-mechanical properties of the synthesized vitrimers were measured using differential scanning calorimetry, thermomechanical analysis, and dynamic mechanical analysis machines.

2.4.1. Differential scanning calorimetry (DSC)

Thermal analysis of the synthesized polymers was performed using a TA Instruments Q2000 Differential Scanning Calorimeter (DSC). The experiments were conducted over a temperature range of −10 °C–250 °C at a heating rate of 5 °C/min under a controlled nitrogen atmosphere. The glass transition temperature (T_g) of the polymers was determined from the second heating cycle, using the tangent method on the heat flow curve. This analysis provides critical insights into the

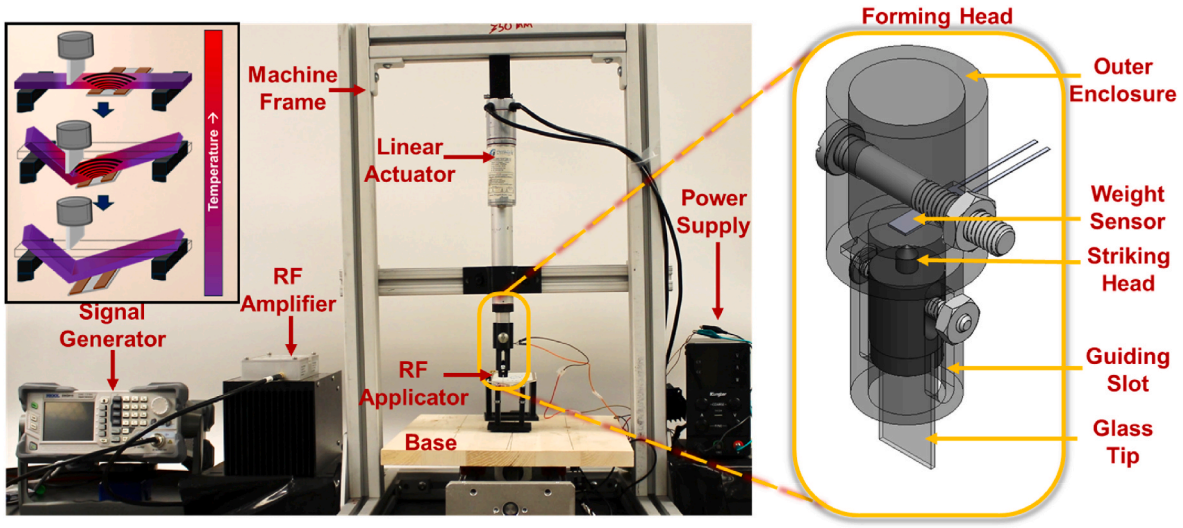

Fig. 1. In-house assembled RF-forming machine showing the signal generated, amplifier, frame, displacement actuator, RF applicator, sample supporting stage, and probe head having load cell sensor, and glass tip. Inset images representative of manufacturing to form/change the dimension of the sample during RF forming.

thermal transitions and stability of the vitrimer systems.

2.4.2. Thermomechanical analysis (TMA)

Thermomechanical properties of the synthesized vitrimers were characterized using a PerkinElmer, TMA7 thermomechanical analysis instrument. Circular disc specimens with a thickness of 2.5–3 mm and a diameter of 4.5 mm were prepared using a precision punching tool. Each sample was subjected to a static mechanical force of 0.1 N, applied via a 6 mm diameter quartz glass probe. The samples were heated at a controlled rate of 5 °C/min, with the temperature range spanning from 0 °C to 300 °C. The topological freezing temperature (T_v) was determined as the temperature at which a significant dimensional change was observed, corresponding to the onset of network rearrangement in the vitrimer material. This parameter provides insight into the thermomechanical stability and processing window of the fabricated vitrimers.

2.4.3. Dynamic mechanical analysis (DMA)

To evaluate the flowability properties of the fabricated vitrimers, non-isothermal creep behaviour was assessed using a Dynamic Mechanical Analyzer (DMA, Electroforce 3200, TA Instruments). Rectangular specimens measuring 30 mm in length and 5 mm in width were cut from the cured vitrimer sheets. The experiments were conducted across a temperature range of 25 °C–250 °C, under a constant applied stress of 0.1 MPa. The thermal transitions were recorded at specific temperatures corresponding to the glass transition temperature (T_g) and the topological freezing temperature (T_v) of the vitrimer samples. These transitions provide insight into the viscoelastic response and thermomechanical flow characteristics of the materials.

2.4.4. Multi-physics simulations

Multi-physics simulation model for RF heating was developed using the Finite Element Method (FEM) via COMSOL Multiphysics 5.5 (Comsol Inc., Boston, MA, USA). The geometry and dimensions of the physical model were based on the RF applicator and polymer setup described earlier. The RF fields were solved using Maxwell's equation:

$$\nabla^2\mathbf{E} = j\omega\mu(\sigma + j\omega\varepsilon)\mathbf{E} \tag{1}$$

where **E** is the electric field (V/m), ω is the angular frequency (rad/s), μ is the permeability, σ is the electric conductivity (S/m), and ε is the complex permittivity.

The complex permittivity ε is given by:

$$\varepsilon = \varepsilon_0\varepsilon_r = \varepsilon_0\left(\varepsilon_r' - j\varepsilon_r''\right) \tag{2}$$

where ε_r' is the relative dielectric constant and ε_r'' is the relative loss factor.

The interaction between the polymer material and the RF fields results in the conversion of electric energy into heat, governed by:

$$P = 2\pi f\varepsilon_0\varepsilon_r''|E|^2 \tag{3}$$

where P is the heat generation (W/m^3), and f is the RF frequency (Hz), $f = \omega/2\,\pi$.

Heat transfer within the polymer material is described by the heat conduction equation:

$$\rho C_p\frac{\partial T}{\partial t} = \nabla\cdot(k\nabla T) + P \tag{4}$$

where ρ is the density (kg/m3), C_p is the specific heat (J/(kg•K)), T is temperature (°C), t is time (s), and k is the thermal conductivity (W/(m•K)).

The heat transfer boundary condition is:

$$-k\frac{\partial T}{\partial n} = h(T_s - T_\infty) \tag{5}$$

where T_s is the polymer surface temperature (°C), T_∞ is the air temperature (~20 °C), and h is the convective heat transfer coefficient (W/(m^{2}K)). The value of h was determined by comparing the simulated cooling curve with experimental cooling data of the polymer after RF heating. Various values of h values were tested, and the best agreement was achieved at h = 15 W/(m^{2}K) (as illustrated in Fig. S4), which was used in all RF heating simulations

To simulate the RF heating of vitrimer materials with three CB concentrations (0.5 %, 3 %, and 5 % by weight), corresponding electrical conductivity values of σ = 0.02, 0.2, and 2 S/m were used as model inputs. The electric conductivity values were extrapolated from Anas et al. [41] The thermal properties of the vitrimer materials, including density, thermal conductivity, and specific heat, were obtained from Vashisth et al. [34]

3. RESULTS and discussions

3.1. Polymer synthesis and characterization

The success of the RF-forming process relies on the thermomechanical properties of the polymer, particularly the ability of polymer chains to extend, mobilize, or slide under controlled loads. Unlike traditional shape memory polymers, vitrimers exhibit flow behaviour through reversible dynamic bond exchange reactions without relying on melting. During RF-forming, applying RF heating and pressure induces molecular chain mobility, and the stress points facilitate bond exchange reactions. This results in permanent deformation, enabling the formation of parts with stable structures that retain their integrity above their service temperature. To assess the viscoelastic properties required for RF-forming, we synthesized two different vitrimers with tailored T_g by adjusting their molecular structures in the crosslinked network (Fig. 2). The first vitrimer, termed V-Low, was synthesized using only bifunctional epoxide and adipic acid with TBD catalyst, whereas the second vitrimer, V-High, was created using a 50:50 mixture of tetra-functional and bifunctional epoxides with adipic acid as the crosslinker, resulting in a more rigid network (Fig. 2c). Both synthesized vitrimers (Fig. 2d and e) contain ester linkages capable of undergoing reversible transesterification reactions in the covalent adaptable network under external stimuli such as temperature and pressure. This makes them suitable for reprocessing and advanced manufacturing using RF-forming.

To understand the viscoelastic and flow behaviour of the synthesized vitrimers, we conducted TMA characterization under a load of 100 mN over a temperature range of 0 °C–300 °C (Fig. 3a). The first thermal transition is seen in form of T_g, this is at observed at 87 °C for V-High and 43 °C for V-Low, indicating higher chain rigidity for vitrimer consisting of tetrafunctional epoxide. This increase in T_g for V-High (80 °C) relative to V-Low (51 °C) was also confirmed by DSC scans (Fig. 3b). Furthermore, V-High demonstrated a significantly higher topological freezing temperature (T_v) of 248 °C, suggesting restricted polymer chain mobility due to the incorporation of tetra-functional epoxides, which render the network stiffer. In contrast, V-Low vitrimers exhibited a lower T_v, indicating easier flowability. The reprocessability of V-High was further evaluated through welding and healability experiments (Fig. S5), while the healing properties of V-Low have been demonstrated in our previous work. The minimal dimensional expansion with increased temperature observed for the tetra-functional epoxide-containing vitrimers indicates that the closely packed crosslinked networks make them more rigid than V-Low.

Next, we examined the creep performance of these polymers through non-isothermal creep experiments. V-High was observed to be stiffer and less flowable as compared to V-Low at similar temperatures (Fig. 3a and b). For non-isothermal creep at 0.1 MPa and 0.5 MPa stresses, we see sharp transitions at 59 °C and 71 °C for V-Low, whereas similar transitions are observed at 85 °C and 85 °C for V-High, respectively. This suggests that vitrimers containing multifunctional epoxides like tetra-functional epoxides require more energy input—in terms of

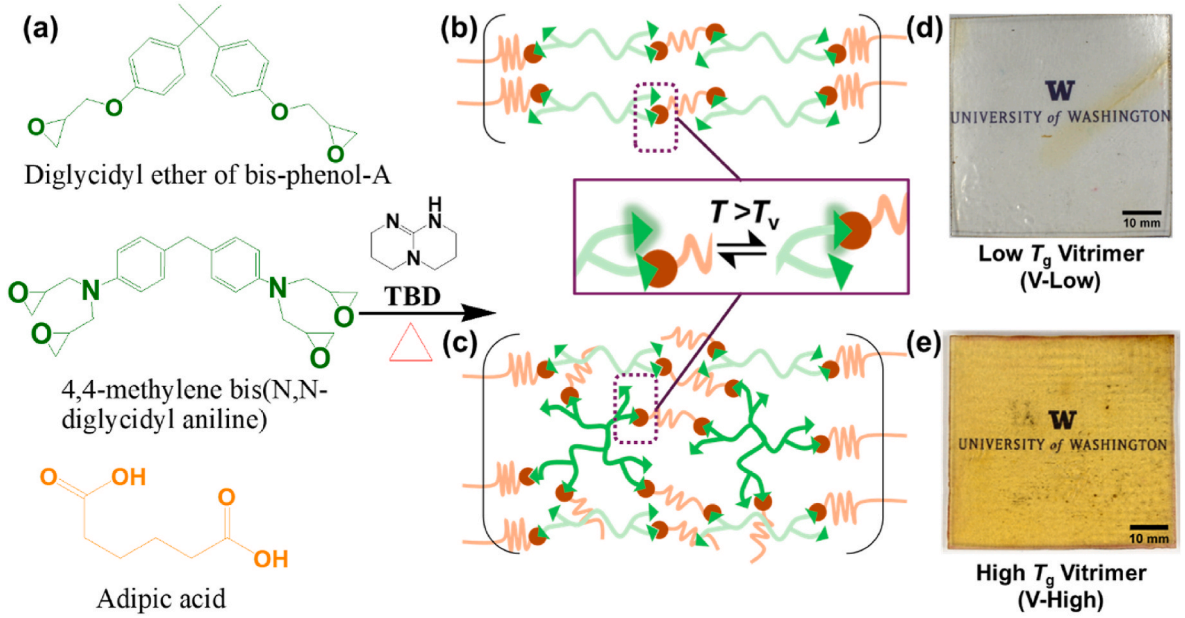

Fig. 2. Synthesis of vitrimers with low and high T_g with (a) chemicals used for synthesis, (b) & (c) schematic for the crosslinked networks and inset for the reversible transesterification reaction mechanism in CANs, and (d) & (e) cured vitrimer plates for the low and high T_g termed as V-Low and V-high respectively.

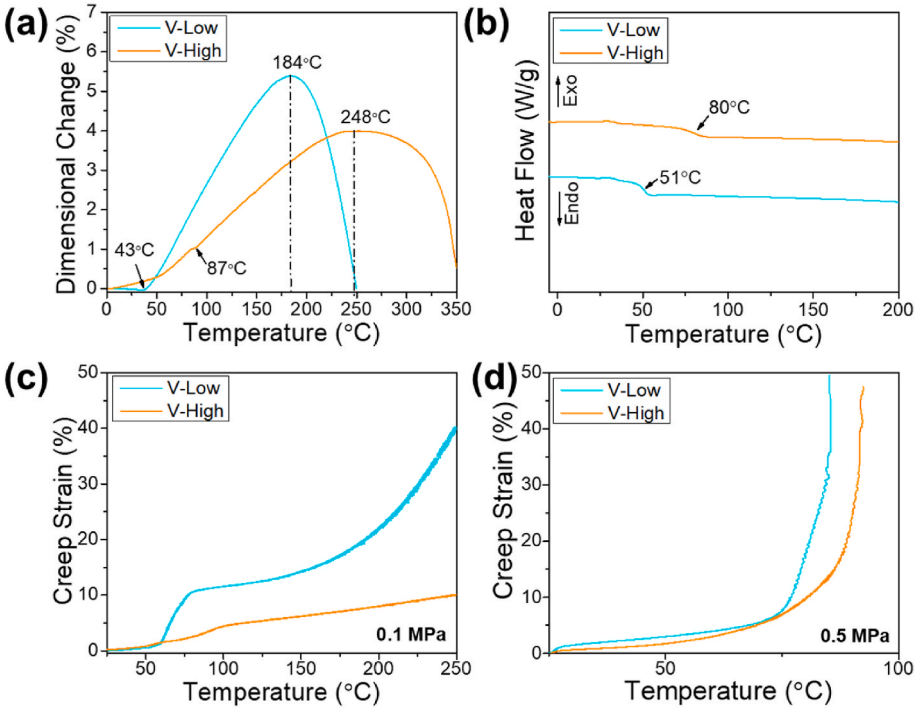

Fig. 3. Thermomechanical properties for the vitrimers showing (a) transition temperatures from TMA including T_g and T_v for the vitrimers, and (b) DSC scans showing T_g for the vitrimers; and (c) & (d) non-isothermal transitions at 0.1 MPa and 0.5 MPa respectively.

temperature and pressure—to undergo deformation. Interestingly, increased stress for V-High does not change the inflection in the strain-temperature curve. This increased energy requirement contributes to more stable molecular structures and, consequently, to the stability of the deformed parts or shapes once formed.

3.2. Optimizing composites for RF heating

To enable efficient RF-forming of vitrimer composites, we optimized the CB content to achieve the best heating response under RF fields. Composites were prepared by incorporating CB into the V-Low vitrimer matrix at concentrations ranging from 0.1 wt% to 5 wt%. The heating response of these composites was evaluated using RF heating at a power input of 5 W and a frequency of 150 MHz (Fig. 4 & Fig. S6). The optimal CB content was determined based on the heating rate (dT/dt) and the maximum achievable temperature within 3 min. Our results show that vitrimers containing 3 wt% CB exhibited the highest heating rates and temperatures. Average heating rates of 2.12 °C/s was observed for 3 wt % samples and a maximum temperature of 205 °C was observed after 3 min of RF exposure. The part of the specimen above the applicator heats

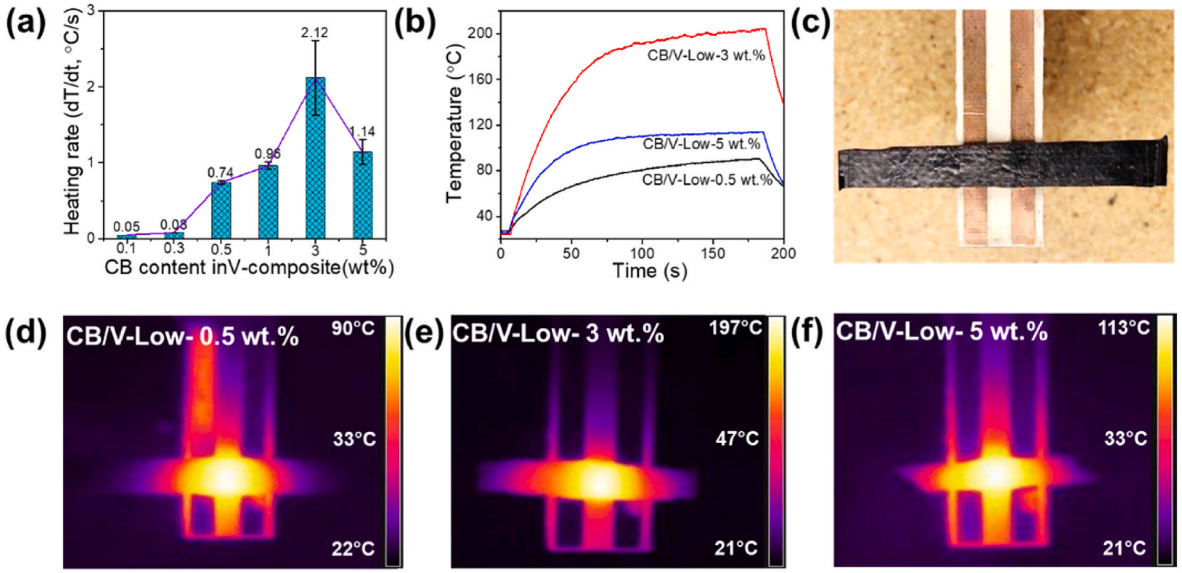

Fig. 4. RF heating response of the carbon black containing vitrimer composites (a) optimization of the CB content 3 wt% in vitrimer samples, (b) measured temperature using 5 W at 150 MHz, (c)sample set up on RF applicator image taken using FLIR camera, (d), (e), & (f) FLIR temperature profiles during the heating at 3 min.

up rapidly, and after RF is switched off the thermal energy distributes over through the length of the specimen.

At 3 wt% concentration, the CB particles are well-dispersed within the vitrimer matrix, developing an optimal network that efficiently absorbs RF energy and dissipates it in form of thermal energy. Above 3 wt % CB, the composites starts reflecting some of the RF energy, leading to decreased heating efficiency [41]. Following optimization, vitrimer plates containing 3 wt% CB were prepared (Fig. S7) for both V-Low and V-High systems, as detailed in Table 1. These plates, with a thickness of approximately ~2.5 mm, were stored in a desiccator for subsequent characterization and RF-forming experiments.

To understand the thermomechanical behaviour of these CB-based

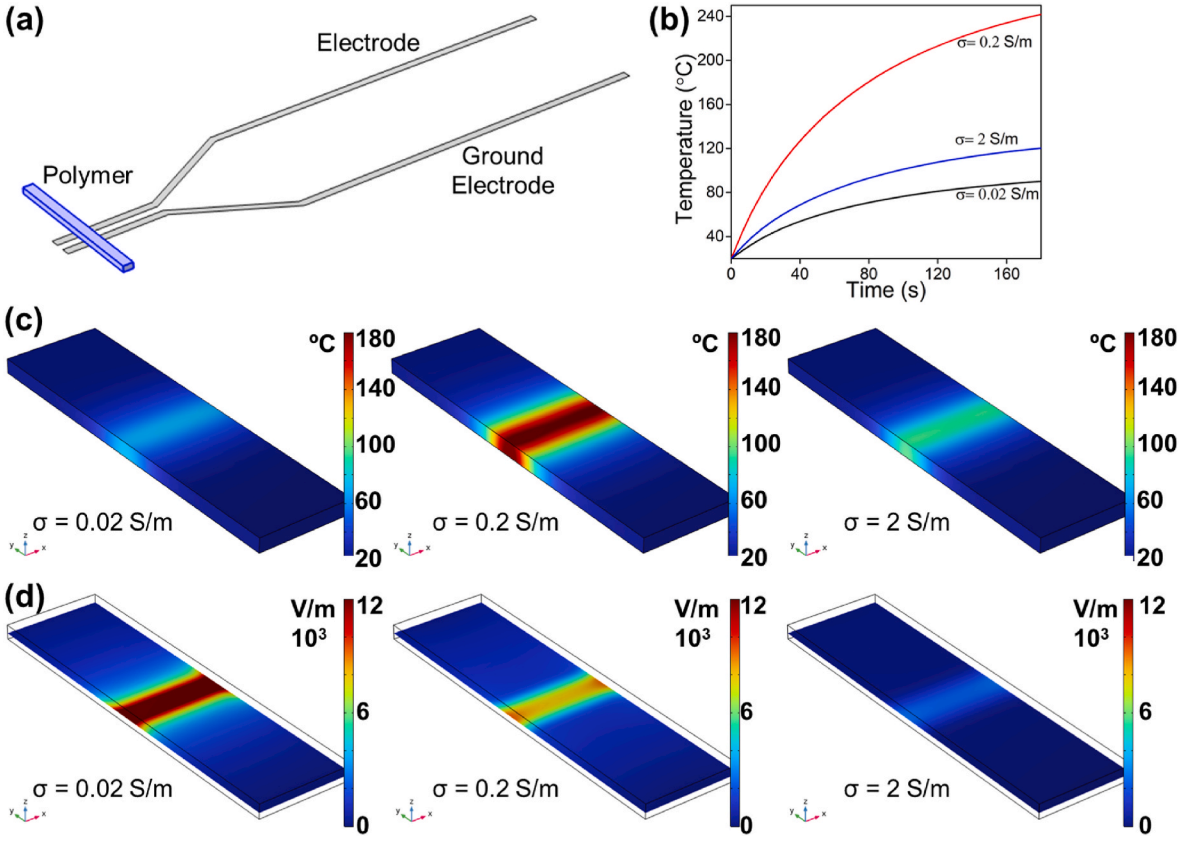

Fig. 5. (a) Geometry model used in COMSOL, (b) simulated temperature vs. time and (c) surface temperature distributions (°C) of the materials with three electric conductivity values (σ = 0.02, 0.2, and 2 S/m) after 3-min RF heating, and (d) simulated electric field distribution (V/m) within the materials.

vitrimer composites, we conducted TMA characterization (Fig. S8). We observed that the T_g for CB/V-Low and CB/V-High were 51 °C and 84 °C, respectively, which are consistent with the values for the pristine V-Low (51 °C) and slightly lower for V-High (87 °C) samples. Notably, both CB/V-Low and CB/V-High exhibited decreased percentages of dimensional change compared to their pristine counterparts, indicating that the incorporation of CB reduces thermal expansion and enhances dimensional stability during processing. However, the peaks for change in dimension vs temperature from TMA experiments broadened compared to the pristine samples suggesting a wider processing window for the vitrimers. Before RF-forming, the optimized CB-containing vitrimer composites were cut to dimensions of 70 mm × 5 mm × 2.5 mm (l × w × t) using an abrasive belt saw and polished on a belt grinder.

3.3. Multi-physics simulations

Fig. 5 shows the multi-physics simulation results of RF heating for vitrimer materials with three different electrical conductivity values representing the dielectric, percolated, and conductive nature of nano-reinforced polymers (σ = 0.02, 0.2, and 2 S/m). The simulated surface temperature distributions (Fig. 5b) matched closely with the experimental results for all three CB concentrations (Fig. 4), demonstrating the ability of the simulation model to predict RF heating behaviour across different materials. The results also demonstrate that the electric fields and the resulting heat generation were concentrated in the region of the material between the two electrodes. The localized heating is attributed to the fringing field effect, caused by the strong electric field distribution near the electrodes. Such localization enhances the efficiency and precision of RF heating, making it an effective processing method where targeted heating is required.

The simulations further illustrate how variations in electrical conductivity affect the intensity of the electric field and, consequently, the RF heating rate. Among the three materials, the sample with intermediate conductivity (σ = 0.2 S/m) had the most efficient RF heating, achieving the highest heating rate under identical conditions (RF power and frequency).

The heating rate ($\frac{\Delta T}{\Delta t}$) depends on the absorbed RF energy (P) and the specific heat of the material, as expressed in the energy balance equation (SI Eq. (1)):

Assuming the vitrimer materials have the same mass (m) and specific heat (C_p), the RF heating rate is directly proportional to the absorbed RF energy (P), which itself is proportional to the dielectric loss factor ε_r'' and the square of the electric field intensity ($|E|^2$) (Eq. (3)).

The dielectric loss factor comprises contributions from polarization losses (ε_p'') and conductivity losses (ε_σ'') [42]:

$$\varepsilon_r'' = \varepsilon_p'' + \varepsilon_\sigma'' = \varepsilon_p'' + \frac{\sigma}{2\pi f \varepsilon_0} \tag{6}$$

For vitrimer materials containing CB, orientation polarization is negligible compared to conductivity losses [41,43] that is ($\varepsilon_d'' = 0$). As a result, the loss factor simplifies to:

$$\varepsilon_r'' = \frac{\sigma}{2\pi f \varepsilon_0} \tag{7}$$

Substituting into Equation (3), the absorbed RF energy becomes:

$$P = 2\pi f \varepsilon_0 \varepsilon_r'' |E|^2 = 2\pi f \varepsilon_0 \frac{\sigma}{2\pi f \varepsilon_0} |E|^2 = \sigma \left|E\right|^2 \tag{8}$$

The simulation results indicate that the average electric field intensity (E) was approximately 12,000, 7,000, and 1500 V/m for the vitrimer materials with σ = 0.02, 0.2, and 2 S/m, respectively. That is, the larger electricity conductivity of the polymers with higher concentration of CB reduced the electric field intensity in the heated sample. Using the relationship $\sigma|E|^2$ and the 3 wt% CB polymer as the reference the ratios of absorbed RF energy (P) for the three materials were calculated as 0.3:1:0.5 (Table 2). These ratios explain why the material with σ = 0.2 S/m (3 % CB) had the highest heating rates, followed by σ = 2 S/m and σ = 0.02 S/m. The theoretical calculation is consistent with the experimental result in Fig. 4. Table 2 highlights the important role of electrical conductivity and electric field intensity in RF heating of vitrimer.

These results show that an optimal dispersion achieved at a 3 wt% filler concentration creates a balanced network where the conductivity is sufficient to absorb RF energy effectively without overly dampening the electric field.

3.4. RF-forming and composites assembly

Using RF heating response of 3 wt% CB vitrimer samples, we performed RF-forming on composites to make complex shapes. Fig. 6a–g illustrates the RF-forming process carried out with the custom-built RF forming machine. The vitrimer samples were roller-supported at both ends using a 3D-printed attachment integrated into the RF applicator. The actuator probe was aligned with the sample at the designated heating area, and the necessary displacement was applied after the sample reached a temperature of T_g + 20 °C and was sufficiently softened for deformation. A temperature above the T_g was chosen to ensure that the molecular chains gain enough thermal energy to transition from a rigid, glassy state to a more flexible, rubbery state, allowing increased chain mobility and segmental motion.

The forming process was conducted using the optimized frequency of 150 MHz, while the RF power input varied between 5 and 10 W to achieve the required deformation temperatures—70 °C for CB/V-Low and 110 °C for CB/V-High vitrimer samples. The temperature requirement is similar to conventional thermoforming in which the temperature must exceed the material's T_g or heat deflection temperature to reach the rubbery state, enabling deformation under an external load [28,44]. In our work, the vitrimer samples were loaded above their T_g values, ensuring sufficient flowability with minimal load.

The applied force and displacement response from the actuator during RF-forming were recorded, as shown in Fig. 6h and i. For CB/V-Low, a total displacement of ~10 mm was applied once the temperature reached 70 °C, and a resulting reaction force of 564 mN was observed (Fig. 6h). Similarly, the CB/V-High system, was first heated to 110 °C and then the actuator was extended by ~10 mm resulting in an initial reaction force of 1181 mN; this higher reaction force was observed due to increased polymeric rigidity (Figs. 6i and S9). Additionally, it can be observed that after RF is switched off and the system starts to cool, the polymeric system relaxes and the reaction force decreases. The force and displacements quantify the influence of vitrimer composition on the RF-forming parameters, with V-High composites requiring more energy to deform due to their stiffer network and thermal properties. The versatility of the RF-forming machine was further demonstrated by creating complex geometries using incremental indentation. For example, a U-shaped structure was formed by sequentially indenting at three pre-designated points along the sample, demonstrating the flexibility of this process in achieving intricate geometries without using traditional molds (Fig. 7a and Fig. S10). This indicates that the RF-forming setup, with further enhancement in tooling design, could be beneficial for more advanced and incremental forming applications in viscoelastic

Table 2
Values in calculating RF heating rates of vitrimer materials.

Vitrimer	σ (S/m)	E (V/m)	Normalized[a] σE^2	Normalized $\frac{\Delta T}{\Delta t}$
CB-V 0.5 %	0.02	12,000	0.3	0.3
CB-V 3 %	0.2	7000	1	1
CB-V 5 %	2	1500	0.5	0.5

[a] Normalized: Values were obtained by dividing each value by the corresponding reference value for CB-V 3 %.

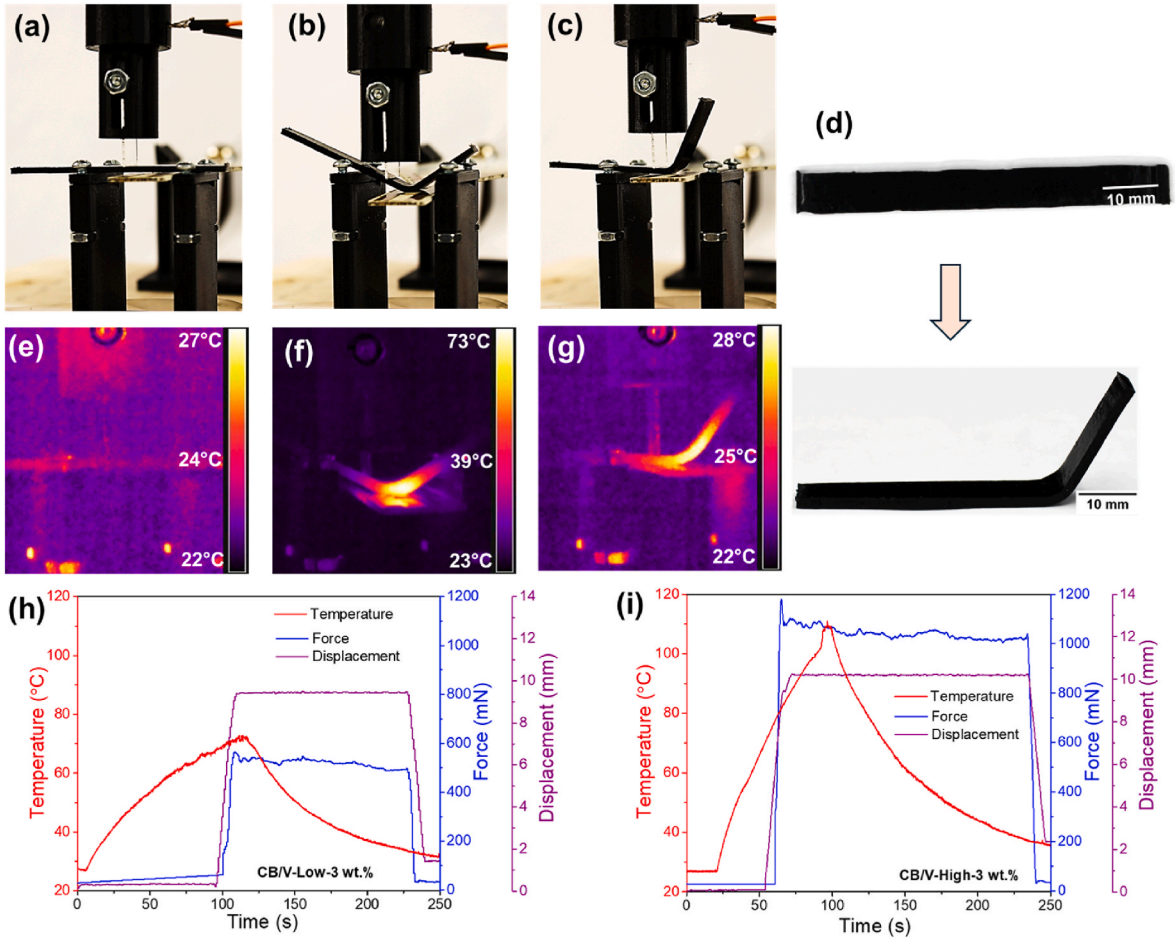

Fig. 6. Manufacturing process during the structural forming of the vitrimer samples (a–c) deformation stages, (d) transformed structure from straight sample to a formed structure, (e–f) FLIR images showing temperature during the process, (h) & (i) observed temperatures, voltages, and load during the forming of vitrimer samples V-Low and V-High respectively.

materials.

Next, we explored the energy-efficient RF heating method for welding and assembling parts composed of CB-based vitrimer composites. RF heating was applied to the edges of previously RF-formed CB/V-Low and CB/V-High samples to achieve a hybrid weld between two materials with distinct vitrimer chemistries and material properties. Fig. 7 shows the assembly process of the two RF-formed parts into a complex “W" shape, representing the initials of the University of Washington. The welding process was conducted by stacking the CB/V-High part with a higher T_v value closer to the RF applicator, while the CB/V-Low part was positioned on top. This configuration ensured that each part reached its respective flow temperatures for effective welding. The RF heating process was carried out at ~236 °C (close to the T_v of CB/V-High), resulting in an interfacial temperature of 220 °C for CB/V-Low, which enabled the rearrangement reaction at the interface. The welding process was maintained for 10 min, followed by 5 min of cooling while holding the parts in position for consolidation, ultimately resulting in a free-standing W-shaped bonded structure (Fig. 7b). This successful welding highlights the utility of RF heating for creating stable, bonded structures between vitrimers with different thermal properties. Additionally, this shows that localized heating through RF can initiate bond exchange reaction in vitrimers at a local interface and weld the material without full volumetric oven heating.

The demonstrated RF-forming approach advances the scientific understanding of vitrimer processing and holds significant promise for industrial applications. By harnessing localized RF heating, this method enables rapid, energy-efficient processing without custom molds or dies, thereby reducing both production costs and lead times. Such a moldless, flexible approach is particularly attractive for industries requiring fast prototyping, on-demand manufacturing, and repair of high-performance components—such as automotive, aerospace, and consumer electronics. Moreover, the modular design of the RF-forming system suggests straightforward integration into automated production lines, facilitating scalability from laboratory-scale experiments to full-scale industrial operations. Future work that incorporates real-time process monitoring and further optimization of RF parameters is expected to enhance process reproducibility and throughput, ultimately paving the way for broader adoption of RF-enabled vitrimer forming in advanced manufacturing environments.

4. Conclusions

This study introduced a novel, energy-efficient RF-forming process for vitrimer composites, demonstrating its effectiveness as an alternative to traditional thermoforming methods. Utilizing a custom-built RF-forming machine, we combined localized RF heating with controlled actuation to achieve moldless manufacturing of complex vitrimer geometries. Two vitrimer systems—V-Low and V-High—were synthesized to explore the effect of molecular structure on thermomechanical properties and RF-forming capabilities. V-High, synthesized with tetrafunctional and bifunctional epoxides, exhibited higher thermal transition temperatures with a T_g of 87 °C and a T_v of 248 °C, compared to V-Low, which showed a T_g of 51 °C and a T_v of 180 °C, reflecting increased rigidity and limited chain mobility. To optimize RF heating efficiency, 3

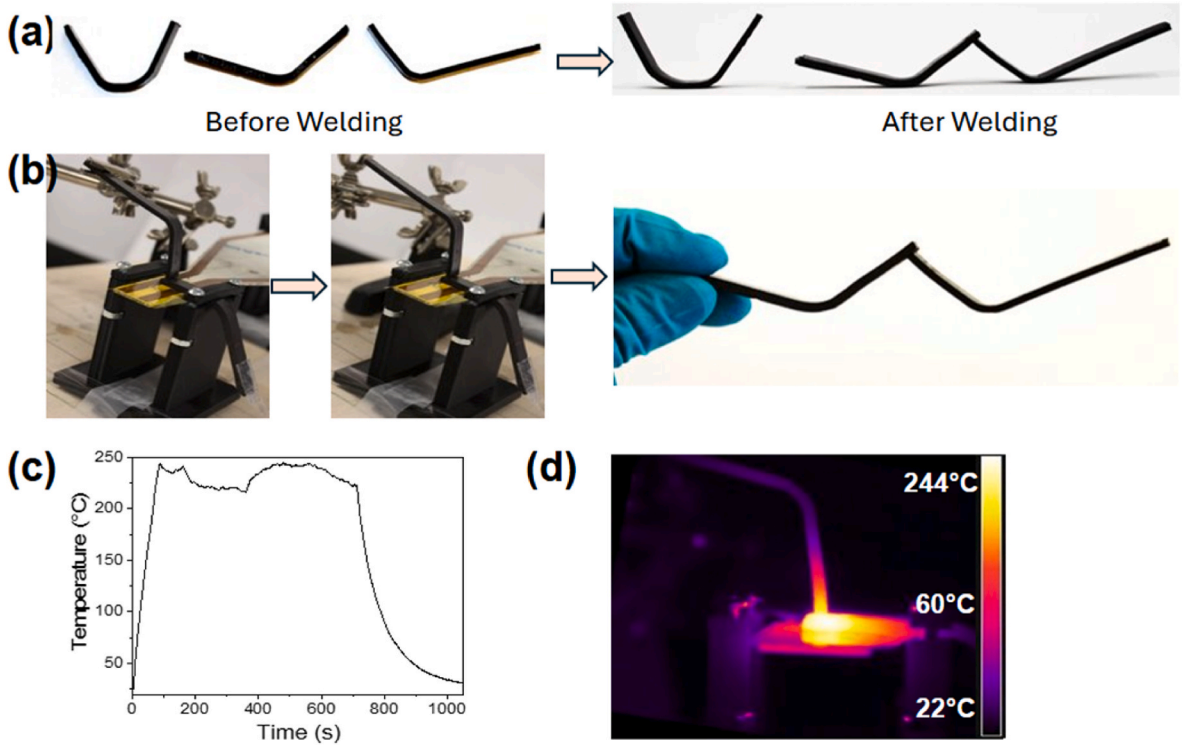

Fig. 7. RF forming used to make (a) shapes U and stretched two half shapes of W from V-Low and V-High vitrimers and welded together using RF, (b) the welding setup and process using RF applicator to bond two halves of the W, and (c) the thermal profile during the welding process and (d) FLIR thermal snapshot of the multi-vitrimer welding process.

wt% CB was incorporated into the vitrimer composites, providing the optimal balance between RF absorption and heating efficiency. Composites with 3 wt% CB achieved average heating rates of 2.12 °C/s with only 5 W of input RF power and reached a maximum temperature of 205 °C within 3 min of RF exposure. Above 3 wt% CB, heating efficiency declined due to excessive conductivity and reduced RF absorption. The multi-physics simulation provides theoretical explanations as why vitrimer materials with 3 wt% CB show the highest heating rate, as compared to the two other CB concentrations in this study. The ability of the RF-forming machine to precisely control heating and deformation enabled successful reshaping of vitrimer samples. Specifically, CB/V-Low and CB/V-High composites were deformed at temperatures of 70 °C and 110 °C respectively, with applied loads of approximately 564 N and 1181 N, to form similar geometries. Finally, these vitrimers (V-high and V-low) were successfully welded together using RF heating to showcase the weldability of two different transesterification vitrimers.

Compared to conventional heating methods, the RF-forming process minimizes energy consumption and eliminates the need for molds, thereby reducing cost and complexity. The resulting vitrimer structures maintained their crosslink density and structural integrity. The versatility of RF-forming for vitrimer composites and its energy efficiency makes it a promising solution for advanced manufacturing applications, particularly where reprocessability, material stability, and moldless fabrication are desirable. Future work will explore the scalability of RF-forming for larger structures, optimize RF parameters to enhance heating efficiency further and evaluate the method's applicability to other dynamic covalent network systems.

CRediT authorship contribution statement

Agni K. Biswal: Writing – review & editing, Methodology, Investigation, Formal analysis. **Surabhit Gupta:** Writing – review & editing, Methodology, Investigation, Formal analysis. **Xu Zhou:** Writing – review & editing, Investigation. **Thomas K. Lewis:** Methodology. **Juming Tang:** Writing – review & editing, Supervision. **Aniruddh Vashisth:** Writing – review & editing, Supervision, Conceptualization.

Declaration of competing interest

The authors declare the following financial interests/personal relationships which may be considered as potential competing interestsAniruddh Vashisth reports was provided by University of Washington. If there are other authors, they declare that they have no known competing financial interests or personal relationships that could have appeared to influence the work reported in this paper.

Acknowledgments

The authors would like to acknowledge the support of the Department of Mechanical Engineering at the University of Washington, Seattle. We would also like to thank the Microsoft Climate Research Initiative and Amazon Research Awards.

Appendix A. Supplementary data

Supplementary data to this article can be found online at https://doi.org/10.1016/j.carbon.2025.120304.

References

[1] Market Value of Composite Materials Worldwide from 2015 to 2028, Statista Research Department, 2023.
[2] K.M. Razeeb, E. Dalton, G.L.W. Cross, A.J. Robinson, Present and future thermal interface materials for electronic devices, Int. Mater. Rev. 63 (2018) 1–21, https://doi.org/10.1080/09506608.2017.1296605.
[3] K. Janeczek, Composite materials for printed electronics in internet of Things applications, Bull. Mater. Sci. 43 (2020) 124, https://doi.org/10.1007/s12034-020-02101-x.
[4] C.J. Kloxin, C.N. Bowman, Covalent adaptable networks: smart, reconfigurable and responsive network systems, Chem. Soc. Rev. 42 (2013) 7161–7173, https://doi.org/10.1039/C3CS60046G.

[5] C.J. Kloxin, T.F. Scott, B.J. Adzima, C.N. Bowman, Covalent adaptable networks (CANs): a unique paradigm in cross-linked polymers, Macromolecules 43 (2010) 2643–2653, https://doi.org/10.1021/ma902596s.
[6] M.K. McBride, B.T. Worrell, T. Brown, L.M. Cox, N. Sowan, C. Wang, M. Podgorski, A.M. Martinez, C.N. Bowman, Enabling applications of covalent adaptable networks, Annu. Rev. Chem. Biomol. Eng. 10 (2019) 175–198, https://doi.org/10.1146/annurev-chembioeng-060718-030217.
[7] B. Briou, B. Améduri, B. Boutevin, Trends in the Diels–Alder reaction in polymer chemistry, Chem. Soc. Rev. 50 (2021) 11055–11097, https://doi.org/10.1039/D0CS01382J.
[8] B. Krishnakumar, R.V.S.P. Sanka, W.H. Binder, V. Parthasarthy, S. Rana, N. Karak, Vitrimers: associative dynamic covalent adaptive networks in thermoset polymers, Chem. Eng. J. 385 (2020) 123820, https://doi.org/10.1016/j.cej.2019.123820.
[9] W. Zou, J. Dong, Y. Luo, Q. Zhao, T. Xie, Dynamic covalent polymer networks: from old chemistry to modern day innovations, Adv. Mater. 29 (2017) 1606100, https://doi.org/10.1002/adma.201606100.
[10] D. Montarnal, M. Capelot, F. Tournilhac, L. Leibler, Silica-like malleable materials from permanent organic networks, Science 334 (2011) 965–968, https://doi.org/10.1126/science.1212648.
[11] M. Kamble, A. Vashisth, H. Yang, S. Pranompont, C.R. Picu, D. Wang, N. Koratkar, Reversing fatigue in carbon-fiber reinforced vitrimer composites, Carbon 187 (2022) 108–114, https://doi.org/10.1016/j.carbon.2021.10.078.
[12] A. Ruiz De Luzuriaga, R. Martin, N. Markaide, A. Rekondo, G. Cabañero, J. Rodríguez, I. Odriozola, Epoxy resin with exchangeable disulfide crosslinks to obtain reprocessable, repairable and recyclable fiber-reinforced thermoset composites, Mater. Horiz. 3 (2016) 241–247, https://doi.org/10.1039/C6MH00029K.
[13] B. Hendriks, J. Waelkens, J.M. Winne, F.E. Du Prez, Poly(thioether) vitrimers via transalkylation of trialkylsulfonium salts, ACS Macro Lett. 6 (2017) 930–934, https://doi.org/10.1021/acsmacrolett.7b00494.
[14] X. Zhang, L. Lin, H. Zhou, G. Zhou, X. Wang, All-natural chitosan-based polyimine vitrimer with multiple advantages: a novel strategy to solve nondegradable plastic waste pollution, J. Hazard Mater. 465 (2024) 133030, https://doi.org/10.1016/j.jhazmat.2023.133030.
[15] A. Kumar, L.A. Connal, Biobased transesterification vitrimers, Macromol. Rapid Commun. 44 (2023) 2200892, https://doi.org/10.1002/marc.202200892.
[16] B. Krishnakumar, A. Pucci, P.P. Wadgaonkar, I. Kumar, W.H. Binder, S. Rana, Vitrimers based on bio-derived chemicals: overview and future prospects, Chem. Eng. J. 433 (2022) 133261, https://doi.org/10.1016/j.cej.2021.133261.
[17] N. Zheng, Y. Xu, Q. Zhao, T. Xie, Dynamic covalent polymer networks: a molecular platform for designing functions beyond chemical recycling and self-healing, Chem. Rev. 121 (2021) 1716–1745, https://doi.org/10.1021/acs.chemrev.0c00938.
[18] A.M. Hubbard, Y. Ren, A. Sarvestani, C.R. Picu, V. Varshney, D. Nepal, Thermomechanical analysis (TMA) of vitrimers, Polym. Test. 118 (2023) 107877, https://doi.org/10.1016/j.polymertesting.2022.107877.
[19] C. Taplan, M. Guerre, J.M. Winne, F.E. Du Prez, Fast processing of highly crosslinked, low-viscosity vitrimers, Mater. Horiz. 7 (2020) 104–110, https://doi.org/10.1039/C9MH01062A.
[20] F. Snijkers, R. Pasquino, A. Maffezzoli, Curing and viscoelasticity of vitrimers, Soft Matter 13 (2017) 258–268, https://doi.org/10.1039/C6SM00707D.
[21] V. Schenk, K. Labastie, M. Destarac, P. Olivier, M. Guerre, Vitrimer composites: current status and future challenges, Mater. Adv. 3 (2022) 8012–8029, https://doi.org/10.1039/D2MA00654E.
[22] J. Ma, L.E. Porath, M.F. Haque, S. Sett, K.F. Rabbi, S. Nam, N. Miljkovic, C. M. Evans, Ultra-thin self-healing vitrimer coatings for durable hydrophobicity, Nat. Commun. 12 (2021) 5210, https://doi.org/10.1038/s41467-021-25508-4.
[23] A.K. Biswal, A. Nandi, H. Wang, A. Vashisth, Ultrasonic welding of fiber reinforced vitrimer composites, Compos. Sci. Technol. 242 (2023) 110202, https://doi.org/10.1016/j.compscitech.2023.110202.
[24] Q. Shi, C. Jin, Z. Chen, L. An, T. Wang, On the welding of vitrimers: chemistry, mechanics and applications, Adv. Funct. Mater. 33 (2023) 2300288, https://doi.org/10.1002/adfm.202300288.
[25] H. Zhang, J. Cui, G. Hu, B. Zhang, Recycling strategies for vitrimers, Int. J. Soc. Netw. Min. 13 (2022) 367–390, https://doi.org/10.1080/19475411.2022.2087785.
[26] A. Quinteros-Sedano, B. Bresson, N.J. Van Zee, R. Nicolaÿ, Improving the thermomechanical properties and processability of elastomeric vitrimers using thermoreversible organic nanofillers, ACS Mater. Lett. 6 (2024) 877–884, https://doi.org/10.1021/acsmaterialslett.4c00076.
[27] P.-X. Tian, Y.-D. Li, Z. Hu, J.-B. Zeng, Fire-resistant and high-performance epoxy vitrimers for fully recyclable carbon fiber-reinforced composites, Mater. Today Chem. 36 (2024) 101965, https://doi.org/10.1016/j.mtchem.2024.101965.
[28] P.J. Martin, Thermoforming of polymers, in: Advances in Polymer Processing, Elsevier, 2009, pp. 352–383, https://doi.org/10.1533/9781845696429.3.352.
[29] M.-S. Shim, J.-J. Park, The formability of aluminum sheet in incremental forming, J. Mater. Process. Technol. 113 (2001) 654–658, https://doi.org/10.1016/S0924-0136(01)00679-3.
[30] L. Ben Said, The incremental sheet forming; technology, modeling and formability: a brief review, Proc. IME E J. Process Mech. Eng. 236 (2022) 2729–2755, https://doi.org/10.1177/09544089221093306.
[31] S.B.M. Echrif, M. Hrairi, Research and progress in incremental sheet forming processes, Mater. Manuf. Process. 26 (2011) 1404–1414, https://doi.org/10.1080/10426914.2010.544817.
[32] P. Collins, E.M.A. Harkin-Jones, P.J. Martin, The role of tool/sheet contact in plug-assisted thermoforming, Int. Polym. Process. 17 (2002) 361–369, https://doi.org/10.3139/217.1702.
[33] C.B. Sweeney, A.G. Moran, J.T. Gruener, A.M. Strasser, M.J. Pospisil, M.A. Saed, M. J. Green, Radio frequency heating of carbon nanotube composite materials, ACS Appl. Mater. Interfaces 10 (2018) 27252–27259, https://doi.org/10.1021/acsami.8b06268.
[34] A. Vashisth, R.E. Healey, M.J. Pospisil, J.H. Oh, M.J. Green, Continuous processing of pre-pregs using radio frequency heating, Compos. Sci. Technol. 195 (2020) 108211, https://doi.org/10.1016/j.compscitech.2020.108211.
[35] N. Patil, X. Zhao, N.K. Mishra, M.A. Saed, M. Radovic, M.J. Green, Rapid heating of silicon carbide fibers under radio frequency fields and application in curing preceramic polymer composites, ACS Appl. Mater. Interfaces 11 (2019) 46132–46139, https://doi.org/10.1021/acsami.9b14971.
[36] C. Zimmerer, C.S. Mejia, T. Utech, K. Arnhold, A. Janke, J. Wosnitza, Inductive heating using a high-magnetic-field pulse to initiate chemical reactions to generate composite materials, Polymers 11 (2019) 535, https://doi.org/10.3390/polym11030535.
[37] A unified approach to the teaching of electromagnetic heating of industrial materials | semantic scholar, (n.d.). https://www.semanticscholar.org/paper/A-Unified-Approach-to-the-Teaching-of-Heating-of-Metaxas/7674e73519a8a9b95f3f2ee0d14733bbbdea6898 (accessed April 2, 2025).
[38] K. Belkhir, G. Riquet, F. Becquart, Polymer processing under microwaves, Adv. Polym. Technol. 2022 (2022) 3961233, https://doi.org/10.1155/2022/3961233.
[39] A. Vashisth, S.T. Upama, M. Anas, J.-H. Oh, N. Patil, M.J. Green, Radio frequency heating and material processing using carbon susceptors, Nanoscale Adv. 3 (2021) 5255–5264, https://doi.org/10.1039/D1NA00217A.
[40] Z. Zhang, A.K. Biswal, A. Nandi, K. Frost, J.A. Smith, B.H. Nguyen, S. Patel, A. Vashisth, V. Iyer, Recyclable vitrimer-based printed circuit boards for sustainable electronics, Nat. Sustain. 7 (2024) 616–627, https://doi.org/10.1038/s41893-024-01333-7.
[41] M. Anas, M.M. Mustafa, A. Vashisth, E. Barnes, M.A. Saed, L.C. Moores, M.J. Green, Universal patterns of radio-frequency heating in nanomaterial-loaded structures, Appl. Mater. Today 23 (2021) 101044, https://doi.org/10.1016/j.apmt.2021.101044.
[42] A.C. Metaxas, R.J. Meredith, Industrial Microwave Heating, P. peregrinus on Behalf of the, Institution of Electrical Engineers, London, UK, 1983.
[43] G. Zhou, J. Zhang, Z. Wang, N. Ning, Y. Huang, Y. Wei, A novel epoxy vitrimer with low dielectric constant at high-frequency, J. Appl. Polym. Sci. 140 (2023) e53713, https://doi.org/10.1002/app.53713.
[44] P.W. Klein, Fundamentals of Plastics Thermoforming, Springer International Publishing, Cham, 2009, https://doi.org/10.1007/978-3-031-02392-7.